H−π Complexes of Acetylene−Ethylene: A Matrix Isolation and Computational Study

K. Sundararajan, K. Sankaran, and K. S. Viswanathan*

Materials Chemistry Division, Indira Gandhi Centre for Atomic Research, Kalpakkam 603 102, India

Anant D. Kulkarni and Shridhar R. Gadre*

Department of Chemistry, University of Pune, Pune-411007, India

Received: June 27, 2001; In Final Form: October 29, 2001

Hydrogen-bonded H···π complexes of C_2H_2 and C_2H_4 were studied both computationally and experimentally. Computationally, C_2H_2–C_2H_4 clusters ranging from 1:1 to 6:1 stoichiometries were identified. Using matrix isolation infrared spectroscopy, the 1:1 adduct was studied in an argon matrix. Formation of these adducts was evidenced by shifts in the vibrational frequencies of the acetylene and ethylene submolecules in the complex. The molecular structure, vibrational frequencies, and stabilization energies of the complexes were calculated at the HF, MP2, MP2(full), and B3LYP levels of theory by employing basis sets ranging from 6-31G(d,p) to 6-311++G(2d,2p). Both computations and experiments showed that two types of complexes are formed, one in which acetylene acts as a proton donor to the π cloud of ethylene and another in which ethylene acts as the proton donor to the π cloud of acetylene. Structures, interaction energies, and vibrational frequencies have also been obtained for 1:2, 1:4, and 1:6 complexes of ethylene and acetylene. This work presents a case study of hydrogen-bonded clusters formed through the H−π interaction.

Introduction

Hydrogen bonding has generated substantial interest given its relevance in the field of chemistry and biology.[1,2] Depending upon the nature of interaction, the strength of the hydrogen bond can vary from well over 10 kcal/mol (termed as strong H-bonds) to instances where the interaction can be barely 1 kcal/mol (weak H-bonds). The strong H-bonding generally occur when a hydrogen attached to an electronegative atom (O or N) interacts with another electronegative atom or a negative ion. Wherever present, the strong H-bonded interactions will often strongly influence many chemical and biochemical phenomena; however, a complete understanding of many chemical and biochemical processes will often demand a complete understanding of the weaker interactions too. It is therefore not surprising that a great deal of interest has been generated in the study of weak H-bond intermolecular interactions. Under the class of the weak H-bonds, the C−H···π systems form a separate class and have received a great deal of attention in recent times. The C−H···π systems present an interesting phenomenon for two reasons. First, unlike conventional hydrogen bonded systems where the hydrogen involved in the H-bonding is attached to an electronegative atom, here the hydrogen is attached to a carbon atom. Not surprisingly, the hybridization of the carbon atom plays an important role, as it significantly determines the acidity of the hydrogens attached to it and hence its ability to form H-bonds. Second, in conventional H-bonded systems, the proton acceptor is an electronegative atom or ion, such as oxygen, nitrogen, and second- and third-row donor atoms.[3−6] However, in the C−H···π systems, the proton acceptor is the π electron system.[7] The original suggestion that π bonds could serve as proton acceptors in H-bonded interactions was made by Dewar[8] and dates back to 1944, though only in recent times has this view been put to a great deal of experimental and computational test. For examples, the interactions between acetylene and hydrogen halides and chloroform clearly involve the π-electrons of acetylene as the proton-accepting site.[9,10] Likewise, the H-bonds involving the π-electrons of ethylene and aromatic systems are also reported.[11−15]

The study of C−H···π H-bonds has generated great interest in recent times, as these interactions appear to be the driving force in the packing of a number of organic crystals and proteins.[16,17] The C−H···π interactions are also believed to be important in molecular recognition.[16] Given the importance of this interaction in a number of chemical and biochemical phenomena, it is imperative to understand the origin of these interactions from a theoretical standpoint and also to generate experimental data on small systems where theories can be put to test. A number of studies are available in the literature involving C−H···π interactions, and they primarily involve the π cloud of ethylene, acetylene, or aromatic ring systems.[9−18]

In this study, we present our results on the acetylene−ethylene H−π system. The study of such weak intermolecular interactions are usually conducted in cold, isolated molecule conditions, such as those that exist in matrix isolation or supersonic beam experiments. We have used matrix isolation infrared spectroscopy to identify and characterize the 1:1 complex of acetylene−ethylene. In the computation of the structure of these acetylene−ethylene complexes, we have used the concept of molecular electrostatic potential (MESP) which greatly aids in predicting sites of attack in a molecule. We believe such aids are essential in deciding structures of larger clusters, such as those encountered in organic and bioorganic crystals. Furthermore, the use of the MESP lays a platform for understanding molecular recognition. In an effort to demonstrate such a utility of MESP, we have in this work extended our computational study beyond 1:1 complexes, to involve higher complexes of acetylene and

* Corresponding authors. E-mail: S.R.G., gadre@chem.unipune.ernet.in; K.S.V., vish@igcar.ernet.in.

10.1021/jp012457g CCC: $22.00
Published on Web 02/02/2002

ethylene; the largest cluster discussed is a 1:6 ethylene−acetylene complex.

Experimental Section

Matrix isolation experiments were performed using a Leybold Heraeus closed-cycle helium compressor cooled cryostat. The cryostat was housed in a vacuum chamber where the base pressure was $< 10^{-6}$ Torr. The details of the vacuum system and related experimental setup have been described elsewhere.[19]

Acetylene (commercial grade, Asiatic Oxygen Limited, Chennai, India) and ethylene (99% pure, Air Products Limited, London) were chilled separately to temperatures of about 170 K and then pumped to eliminate volatile impurities. Acetylene, ethylene, and the matrix gas, argon (IOLAR grade I) were mixed in the desired ratios using standard manometric procedures. The $Ar/C_2H_2/C_2H_4$ mixture of the desired composition was then deposited through an effusive nozzle on to the cold KBr substrate mounted on a cryotip. We used matrix-to-sample ratios ranging from 1000:0.1 to 1000:3 for acetylene and 1000:0.3 to 1000:5 for ethylene. A deposition typically lasted for about 30 min at a rate of ≈3 mmol/h.

Infrared spectra of the matrix isolation samples were recorded over the range 4000−400 cm^{-1}, using a BOMEM MB 100 FTIR spectrometer, operated at a resolution of 1 cm^{-1}. The matrix was then warmed to 35 K, maintained at this temperature for about 15 min, and then recooled to 12 K. Spectra of the matrix, thus annealed, were again recorded. All the spectra shown in this paper were those recorded after annealing the matrix. Spectra of acetylene and ethylene deposited individually in the argon matrix have also been recorded.

Computational Methods

The optimized geometries and the wave functions of the individual molecules are calculated using programs GAUSSIAN[20] and GAMESS[21] while topographical analysis is done using the program UNIPROP.[22] The MESP isosurfaces and all the geometries are visualized using the package UNIVIS-2000,[23] an indigenously developed visualization package by Limaye and Gadre.

The electrostatic potential, $V(\mathbf{r})$ generated by a molecule at a point $\mathbf{r}$ is defined as

$$V(\mathbf{r}) = \sum_{A=1}^{N} \frac{Z_A}{|\mathbf{r} - R_A|} - \int \frac{\rho(\mathbf{r}')}{|\mathbf{r}' - \mathbf{r}|} \mathrm{d}^3\mathbf{r}'$$

where the first term represents the contribution due to nuclei with charges Z_A located at R_A while the second term arises due to (the continuous) electronic charge density [$\rho(\mathbf{r})$]. The critical points (CPs) provide valuable information about the structure and the environment of the molecule. The details of the MESP and the CPs can be found elsewhere.[22,24] The starting geometries of the ethylene···acetylene complexes have been fixed considering the complementarity as revealed by the CPs of ethylene and acetylene.

The geometries thus generated are then optimized at RHF, MP2, MP2(full), and B3LYP levels of theory with various basis sets ranging from 6-31G(d,p) to 6-311++G (2d, 2p) using GAUSSIAN[20] and GAMESS.[21] The hybrid Hartree−Fock density functional method, B3LYP, uses the Becke's three parameter nonlocal exchange functional,[25,26] with the nonlocal correlation functional of Lee et al.[27] Optimizations were followed by frequency calculations to enable us to characterize the nature of the stationary points (by checking for imaginary frequencies) and also to assign the experimentally observed frequencies recorded in the matrix isolation experiments. For comparison with the experimental frequencies, we have used the computed analytical frequencies at the B3LYP/6-31++G(d,p) level.

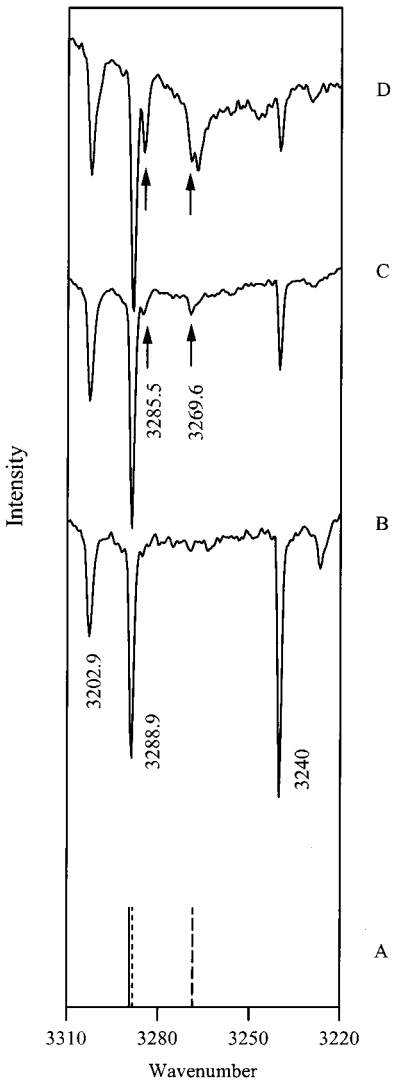

Figure 1. Matrix isolation IR spectra in the region 3310−3220 cm^{-1}: (A) computed stick spectra; (B) C_2H_2−Ar (0.2:1000); (C) C_2H_2−C_2H_4−Ar (0.2:1:1000); (D) C_2H_2−C_2H_4−Ar (0.2:10:1000).

Results and Discussion

Experimental Results. Figures 1 and 2 show the spectra over the regions 3310−3220 and 760−720 cm^{-1}, respectively, obtained when acetylene and ethylene were codeposited in an argon matrix. Also shown in these figures are the spectra obtained when acetylene alone was deposited in an argon matrix.

In the spectral regions mentioned above, C_2H_2 has strong absorptions at 3302.9, 3288.9, and at 736.8 cm^{-1}, which have been assigned to the combination band ($\nu_2 + \nu_4 + \nu_5$), ν_3, and ν_5 modes, respectively.[28] The 3302.9 and 3288.9 cm^{-1} features are in fact Fermi diads involving the ($\nu_2 + \nu_4 + \nu_5$) and ν_3 vibrations. For the discussions in this paper, we will refer to the 3288.9 cm^{-1} feature as ν_3' to indicate the occurrence of the Fermi resonance.[28b] Ethylene has no absorption in this regions.

When acetylene and ethylene were codeposited and the matrix then annealed, product absorption bands appeared at 3285.5, 3269.6, and 749.3 cm^{-1}. These bands appeared *only* when both

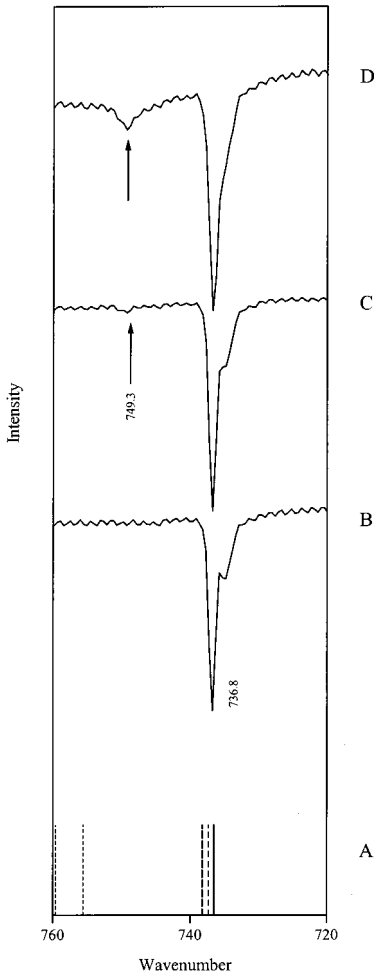

Figure 2. Matrix isolation IR spectra in the region 760−720 cm^{-1}: (A) computed stick spectra; (B) C_2H_2−Ar (0.2:1000); (C) C_2H_2−C_2H_4−Ar (0.2:1:1000); (D) C_2H_2−C_2H_4−Ar (0.2:10:1000).

the reagents were codeposited. Furthermore, these bands increased in intensity as the concentration of either of the two reagents was increased. These observations clearly indicate that these features can be attributed to a complex involving acetylene and ethylene. Since these product bands appeared at low concentrations of acetylene and ethylene, we believe the complex to be of a 1:1 type. The feature at 3269.6 and 3285.5 cm^{-1} can be assigned to the ν_3' mode of the C_2H_2 submolecule in the C_2H_2–C_2H_4 complex. (As discussions in later sections will show, two types of complexes are formed giving rise to two distinct features.) This assignment implies that, following complex formation, the ν_3 mode of the C_2H_2 submolecule is red shifted by 19.3 and 3.4 cm^{-1} from the value obtained for free C_2H_2 for this mode. The feature at 749.3 cm^{-1} can be assigned to the ν_5 mode of the C_2H_2 submolecule in the C_2H_2–C_2H_4 complex.

We also observed a feature due to the C_2H_2–H_2O complex at 3240 cm^{-1},[11] in excellent agreement with that reported in the literature. Features corresponding to a complex involving water appear, as water is an inevitable impurity in a matrix isolation experiment.

Figure 3 shows the infrared spectra over the region 970−940 cm^{-1}, where the C−H bending of ethylene is observed.[11] The ν_7 mode appears at 947.5 cm^{-1} in free ethylene and at 952.7 cm^{-1} in the C_2H_2–C_2H_4 complex. Complex formation has therefore resulted in a 5.2 cm^{-1} blue shift for this mode. Another feature at 959.5 cm^{-1} was also observed, which is due to the C_2H_4–H_2O complex.[11] No feature corresponding to the C−H

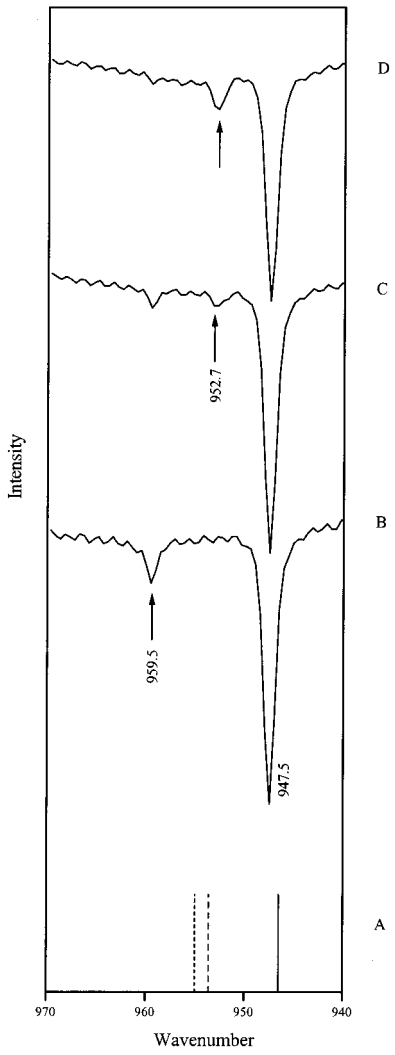

Figure 3. Matrix isolation IR spectra in the region 970−940 cm^{-1}: (A) computed stick spectra; (B) C_2H_4−Ar (0.6:2000); (C) C_2H_2−C_2H_4−Ar (2:0.6:2000); (D) C_2H_2−C_2H_4−Ar (6:0.9:2000).

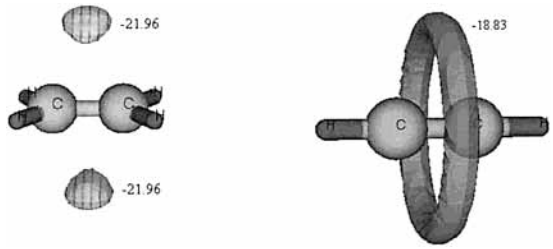

Figure 4. RHF/6-31G(d,p)-optimized geometries of ethylene−acetylene complexes along with negative-valued isosurfaces and the MESP CPs for them.

stretch in the C_2H_4 submolecule in the complex could be observed, probably because its intensity may have been too low to be discerned.

Structure and Energetics of $C_2H_2\cdots C_2H_4$ Complexes. The MESP topography mapping has been carried out for the individual species to understand complementary electrostatic features. As shown in Figure 4 a negative-valued MESP isosurface of ethylene (magnitude −21.96 kcal/mol) is observed above and below the C−C bond of ethylene while a ring of negative valued MESP (magnitude −18.83kcal/mol) is seen around the C−C bond of acetylene. In all the figures the distances are reported in Å while the MESP values are in kcal/mol. The negative valued MESP CPs ((3,+3) CP with magni-

TABLE 1: MESP-Derived Charges of Ethylene, Acetylene, and Ethylene···Acetylene (1:1) Complexes Calculated at RHF/6-31G(d,p)-Optimized Geometries[a]

	MESP-derived charges (atoms)	
molecule	C	H
acetylene (a)	−0.259	0.259
ethylene (e)	−0.280	0.140
1A	−0.237 (a), −0.279 (a), −0.252 (e)	0.234 (a), 0.259 (a), 0.132 (e)
1B	−0.253 (a), −0.249 (a), −0.272 (e), −0.278 (e)	0.258 (a), 0.256 (a), 0.134 (e), 0.132 (e), 0.133 (e), 0.139 (e)

[a] The e and a denote atoms in ethylene and acetylene, respectively. Symmetry-related charges are not reported.

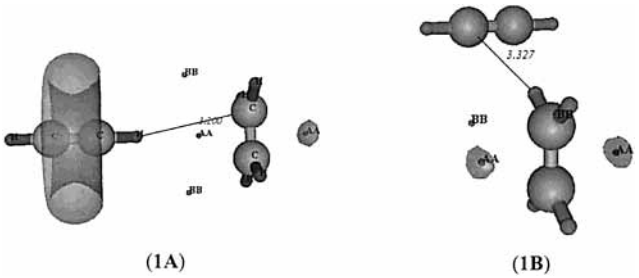

Figure 5. RHF/6-31G(d,p)-optimized geometries of ethylene···acetylene complexes along with negative valued isosurfaces and the MESP CPs for them.

TABLE 2: MESP CPs (Values in kcal/mol) for Ethylene, Acetylene, and Ethylene···(Acetylene)$_n$ (n = 1, 2, 4) Complexes Calculated at RHF/6-31G(d,p)-Optimized Geometries

molecule	MESP (no. of MESP CPs)	nature
acetylene	−24.41	degenerate ring
ethylene	−23.97 (2)	(3,+3)
1A	−19.08, −7.47	(3,+3)
	1.07 (2)	(3,+1)
1B	−25.98 (2)	(3,+3)
	−5.15, −5.02	(3,+1)
2A	−26.04 (2), −23.16, −23.03, −20.65, −9.35	(3,+3)
	−25.67, −22.40, −4.83, −4.58	(3,+1)
	3.20, 2.13, 3.89, 9.35	(3,−1)
2B	−30.49, −20.65 (2), −19.73, −9.22	(3,+3)
	−5.46 (2), −0.56 (2)	(3,+1)
	0.56, 5.84	(3,−1)
4	−25.35 (2), −22.53 (2), −22.34, −7.28 (2)	(3,+3)
	−4.20(2), −21.73, −24.91, −3.83 (2), 1.13	(3,+1)
	4.58 (2), 10.10, 9.98, 4.64	(3,−1)

tude −23.97 kcal/mol) has been observed inside the isosurfaces of ethylene. A look at these MESP features suggests two possible structures for ethylene···acetylene complexes. Structure **1A** (Figure 5) shows the structure of a C_2H_2–C_2H_4 complex in which the hydrogen of acetylene interacts with the π cloud of ethylene forming an H···π complex—a complex where acetylene is the proton donor. Structure **1B** (Figure 5) depicts another possible structure for a H···π complex in which ethylene acts as the proton donor to acetylene. Both structures were found to correspond to minima on the potential surface as verified by vibrational frequency calculations. The distances between the two submolecules in the complexes **1A,B** are shown in Figure 5. The C···H distance in complex **1A** is 3.201 Å at the HF/6-31G(d,p) level and 3.327 Å in the complex **1B** at the same level. These distances are comparable with earlier results reported by Fan et al.[17] and Jemmis et al.[3] for C−H···π interactions. The MESP-derived charges of ethylene, acetylene, and the two complexes **1A,B** calculated at RHF/6-31G(d,p) level are given in Table 1. The formation of the complexes can be inferred from the changes in the net atomic charges in the complex compared with the values in the uncomplexed species. Table 2 gives the MESP critical points and their nature.

TABLE 3: Raw Interaction Energies[a] and Interaction Energies Corrected for ZPE[b] in Parenthesis at HF, B3LYP, and MP2 Levels with the 6-31++G(d,p) Basis Set[c]

	interactn energy (ΔE)		
complex	HF/ 6-31++G(d,p)	B3LYP/ 6-31++G(d,p)	MP2/ 6-31++G(d,p)
1A[d]	−0.82 (−0.39)	−0.97 (−0.42)	−1.98 (−0.90)
1B[d]	−0.27 (−0.071)	−0.28 (−0.0014)	−1.10 (−0.88)

[a] Raw interaction energies refer to energies not corrected for either ZPE or BSSE. [b] The computed ZPE was scaled by 0.92 for HF, 0.94 for B3LYP, and 0.96 for MP2 for the application of the ZPE correction. [c] All the energies are in kcal/mol (see text for details). [d] Mode involving C_2H_2 as a proton donor (**1A**). [e] Mode involving C_2H_2 as a proton acceptor (**1B**).

TABLE 4: Raw Interaction Energies[a] and Interaction Energies Corrected for BSSE (in Parentheses) at HF/6-31++G(d,p), B3LYP/6-31++G(d,p), and MP2/6-311++G(2d,2p) Levels[b]

	interactn energy (ΔE)		
complex	HF/ 6-31++G(d,p)	B3LYP/ 6-31++G(d,p)	MP2/ 6-311++G(2d,2p)
1A[c]	−0.82 (−0.69)	−0.97 (−0.76)	−1.76 (−1.36)
1B[d]	−0.27 (−0.20)	−0.28 (−0.16)	−1.46 (−1.04)

[a] Raw interaction energies refer to energies not corrected for either ZPE or BSSE. [b] All the energies are in kcal/mol (see text for details). [c] Mode involving C_2H_2 as a proton donor (**1A**). [d] Mode involving C_2H_2 as a proton acceptor (**1B**).

Table 3 gives the ZPE-corrected as well as -uncorrected interaction energies for the two complexes, while Table 4 gives BSSE-corrected and -uncorrected interaction energies, computed at the HF, B3LYP, and MP2 levels using various basis sets. At all levels, it can be seen that complex **1A** is more strongly bound than **1B** and not surprisingly so. The formation of complex **1A** is indicated to be weakly exothermic by about 0.8−2.0 kcal/mol at the various levels of theory used (ZPE uncorrected) and drops to about 0.4−0.9 kcal/mol with ZPE correction. At the MP2 (full)/6-31++G(d,p) level, the same complex is indicated to be endothermic (Table S1 in the Supporting Information). Complex **1B** is barely stabilized at the HF and B3LYP levels. At the MP2 (full)/6-31++G(d,p) level this complex too becomes destabilized on the application of ZPE (Table S1 in the Supporting Information). Interestingly both complexes, **1A,B**, are seen in our matrix isolation experiments. It is likely that the barely bound **1B** complex is stabilized in the matrix cage and hence is discernible in our experiments. Such weak complexes would never survive in gas-phase experiments, and the observation of such weak complexes in our experiments is a clear demonstration of the advantage of the matrix isolation technique in locating weak local minima.

A look at Tables 3, 4, and 6 [depicting the interaction energies for the two complexes at HF, MP2, and B3LYP levels using the 6-31G(d,p) and 6-31++G(d,p) basis sets and MP2/6-311++(2d,2p)] brings out the effect of the different basis sets.

TABLE 5: Experimental and B3LYP/6-31++G(d,p) Computed (Scaled) Frequencies, Scaling Factors, and Mode Assignments for 1A and 1B

exptl ν (cm^{-1})	calcd ν (cm^{-1})	scaling factor	mode assgnt
3288.9	3289.4 (93)[a]	0.959	ν_3 of C_2H_2
3269.5	3268.6 (193)	0.959	ν_3 of C_2H_2 in $C_2H_2-C_2H_4$[b]
3285.5	3288.4 (94)	0.959	ν_3 of C_2H_2 in $C_2H_2-C_2H_4$[c]
736.8	736.5 (112)	0.959	ν_5 of C_2H_2
749.5	755.6 (85), 759.6 (97)	0.959	ν_5 of C_2H_2 in $C_2H_2-C_2H_4$[b]
d	737.3 (116), 738.2 (106)	0.959	ν_5 of C_2H_2 in $C_2H_2-C_2H_4$[c]
3111.7	3111.0 (28)	0.959	ν_9 of C_2H_6
d	3111.8 (21)	0.959	ν_9 of C_2H_2 in $C_2H_2-C_2H_4$[b]
d	3110.7 (22)	0.959	ν_9 of C_2H_2 in $C_2H_2-C_2H_4$[c]
947.5	946.5 (119)	0.971	ν_7 of C_2H_4
952.7	955.0 (136)	0.971	ν_7 of C_2H_2 in $C_2H_2-C_2H_4$[b]
d	953.6 (87)	0.971	ν_7 of C_2H_2 in $C_2H_2-C_2H_4$[c]

[a] Computed infrared intensities (km/mol) are given in parentheses. [b] Mode involving C_2H_2 as a proton donor (**1A**). [c] Mode involving C_2H_2 as a proton acceptor (**1B**). [d] Experimentally features are not observed.

Although there are deviations in the numerical values of energies with the different basis sets, the trends in the energetics are found to be qualitatively identical for these complexes. When we applied both the ZPE and BSSE corrections, the interaction energy in a few cases becomes positive, indicating complex formation to be endothermic. However, the combined application of both these corrections has been considered to overcorrect and the actual interaction energies may indeed be more negative.[29,30] Hence, we have not reported the interaction energies inclusive of ZPE + BSSE corrections. It can also be seen that expanding to a basis with diffuse functions leads to a qualitative similar picture with regard to complex stability.

Vibrational Assignments. Vibrational frequencies of the different modes were calculated and compared with the experimentally observed values (Table 5). The computed frequencies were scaled on a mode by mode basis. The scaling factors were obtained by comparing the computed frequencies for the uncomplexed acetylene or ethylene with those obtained experimentally. The scaling factors thus obtained for the different modes of the uncomplexed reagents were then used to scale the computed frequencies in the complex. The scaling factors for the different modes (0.959 for C_2H_2 and 0.971 for C_2H_4) are also given in Table 5. The scaled frequencies (presented in Table 5 and also shown as stick spectra in Figures 1−3) can be seen to agree with those obtained experimentally.

ν_3' Mode of Acetylene. As mentioned earlier, the ν_3' stretch of acetylene submolecule in the complex occurs at 3269.6 and 3285.5 cm^{-1}. The feature at 3269.6 cm^{-1} is assigned to the ν_3' mode in the acetylene submolecule of complex **1A**, which agrees well with the computed value of 3268.6 cm^{-1} for this complex. The 3285.5 cm^{-1} feature is assigned to the acetylene submolecule of complex **1B**, again in agreement with the computed value of 3288.4 cm^{-1}. The good agreement between the experimental and computed values is clear evidence that the complexes **1A,B** are of the H···π type as shown in Figure 5.

It should be noted that the ν_3' mode of the proton-accepting acetylene submolecule in the acetylene dimer also occurs at 3285.2 cm^{-1}, in close proximity to the value of 3285.5 cm^{-1}, which we report for the acetylene−ethylene complex **1B**. It is therefore necessary to rule out the possibility that the 3285 cm^{-1} feature assigned in this work to the heterodimer of acetylene and ethylene is not really due to the acetylene homodimer. We therefore performed experiments with acetylene alone, where the acetylene to matrix (Ar) ratio was 1:10000, at which dilution *no feature* was observed at 3285.2 cm^{-1} (**1B**), clearly indicating that the acetylene homodimer was not formed at this concentration. When ethylene was added to acetylene (maintaining the same acetylene-to-argon ratio), the 3285.5 cm^{-1} peak appeared. Furthermore, this peak grew in intensity as the concentration of ethylene was increased, therefore providing strong evidence that the 3285.5 cm^{-1} feature in the above set of experiments was really due to the acetylene−ethylene heterodimer **1B**.

A consideration of experimental and computed shifts in the ν_3' stretch of the acetylene submolecule in the complexes relative to that in the free acetylene shows a reassuring trend. In complexes where acetylene is a proton donor, the shifts in the ν_3 mode of the acetylene submolecule are usually large. For example, the ν_3' mode of acetylene in the acetylene−water complex is shifted by ≈49 cm^{-1}, where acetylene acts as a proton donor.[31] In complexes where acetylene is the proton acceptor, the shifts in the ν_3' mode of the acetylene submolecule are comparatively small. For example the ν_3' mode of acetylene in the acetylene−chloroform complex is shifted only by 5.9 cm^{-1}, where acetylene is the proton acceptor.[10] In this study, the ν_3' mode of the acetylene submolecule is shifted by 19.3 cm^{-1} in complex **1A** where acetylene is the proton donor and by 3.4 cm^{-1} in complex **1B** where acetylene is the proton acceptor.

ν_5 Mode of Acetylene. The ν_5 mode of the acetylene submolecule in complex **1A** occurs at 749.3 cm^{-1}, which implies a blue shift of 13.7 cm^{-1} from that of the free acetylene feature. No feature was observed for the acetylene submolecule in complex **1B**, as these features probably appear at almost the same place where the free acetylene absorbs, as indicated by our calculations, and hence could not be resolved in our experiments.

ν_7 Mode of Ethylene. The ν_7 mode of the ethylene submolecule in the complex occurs at 952.7 cm^{-1}. The blue shift by 5.2 cm^{-1} in the ν_7 mode of ethylene submolecule in the acetylene−ethylene complex is in good agreement with that computed for the complex. However, the ν_7 modes of ethylene in the two complexes **1A,B** are computed to lie within 1.4 cm^{-1} and we therefore do not assign the experimental feature at 952.7 cm^{-1} specifically to either **1A** or **1B** complex. With such small differences it would be difficult to resolve the features due to each of the complexes. The feature at 959.5 cm^{-1} is due to ethylene−water complex.[11]

Higher Complexes of Acetylene and Ethylene. To find out the possible sites of attack of the next acetylene molecule on ethylene···acetylene complex, MESP topography mapping has been done for RHF optimized structures of **1A,B**. In the case of complex **1A** the MESP minimum of ethylene increases to −19.08 kcal/mol and the minimum around acetylene drops down to −26.98 kcal/mol (isolated acetylene has this minimum of −23.85 kcal/mol), suggesting that the attack of next acetylene molecule will be favorable near acetylene inclined toward ethylene. For complex **1B** the MESP minimum of ethylene drops down to −25.98 kcal/mol while the minimum around acetylene increases to −21.96 kcal/mol. These features suggest that the binding of next acetylene will be favored at the ethylene side perpendicular to the C−C bond. On the basis of these MESP guidelines, five structures, optimized at RHF/6-31G(d,p) level, for the 1:2 ethylene−acetylene structures were derived. Of these structures **2A,B** alone have been shown with their negative-valued MESP isosurfaces in Figure 6 and their interaction energies in Table 6. The MESP-based approach has been extended to predict the various possible geometries of ethylene···(acetylene)$_n$ complexes, $n = 4$ and 6. For complexes **2A,B**, the negative-valued MESP isosurfaces (−12.55 kcal/mol) around

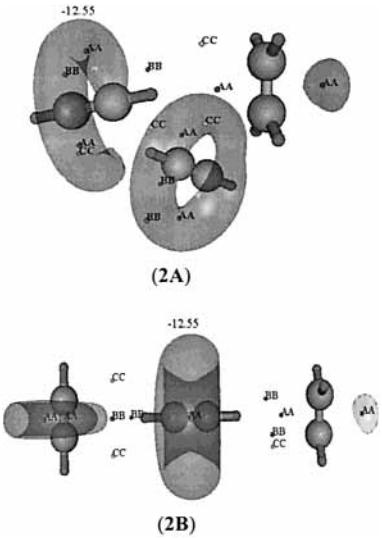

Figure 6. RHF/6-31G(d,p)-optimized geometries of ethylene···(acetylene)$_2$ (**2A,B**) complexes. Negative-valued isosurfaces and the MESP CPs for lowest energy structures have also been shown.

TABLE 6: Ab Initio Interaction Energies (in kcal/mol) (uncorrected for BSSE and ZPE) of Ethylene···(Acetylene)$_n$ Complexes at the RHF/6-31G(d,p), B3LYP/6-31G(d,p), and MP2(Full)/6-31G(d,p) Levels[a]

complex	Δ*E*(RHF)/ 6-31G(d,p)	Δ*E*(B3LYP)/ 6-31G(d,p)	Δ*E*(MP2(full))/ 6-31G(d,p)
1A	−1.418	−1.678	−2.234
1B	−0.552	−0.737	−1.330
2A	−3.232	−3.064	−5.434
2B	−2.629	−1.394	−4.286
4	−6.388	−8.196	
6	−11.232	−14.533	

[a] Structures are depicted in Figures 5−7. See text for details.

acetylene molecules are larger than those for the ethylene molecule and also the MESP values at the CPs are more negative than those for individual moieties, viz. acetylene and ethylene (cf. Table 2). This feature is suggestive of reasonably strong interaction with the next acetylene molecule. Figure 7 shows the MESP isosurface generated at RHF-optimized geometries of ethylene···(acetylene)$_4$ complex (**4**) and the RHF-optimized geometry of ethylene···(acetylene)$_6$ (**6**). Both the structures **4** and **6** are in agreement with the predictions of MESP approach. However, note that the MESP minimum for complex **4** is now smaller in magnitude (−25.35 kcal/mol.)—quite comparable to the MESP minima for the acetylene molecule. Hence, the interaction of an acetylene molecule with complex **4** is expected to be roughly of the same strength as the interaction between acetylene molecules.

Stability of Higher Complexes. To predict the stability and the existence of the higher clusters ethylene···(acetylene)$_n$, a new term, relative interaction energy (ΔE_{rel}), can be defined as follows:

$$\Delta E_{rel} = \Delta E_{e\cdots n(a)} - \Delta E_{n(a)} = E_{e\cdots n(a)} - E_e - E_{n(a)}$$

Here e and a denote ethylene and acetylene molecules, respectively, and *n*(a) is the cluster of *n* acetylenes. The entity ΔE_{rel} is indicative of whether the ethylene molecule can interact favorably with the cluster of *n* acetylenes. A negative value of ΔE_{rel} shows a favorable interaction. The homoclusters of acetylene ($(C_2H_2)_n$) of sizes n = 2, 4, and 6 were used for defining the relative interaction energy. The calculations at RHF/6-311++G (d,p) level for ethylene···(acetylene)$_n$ complexes

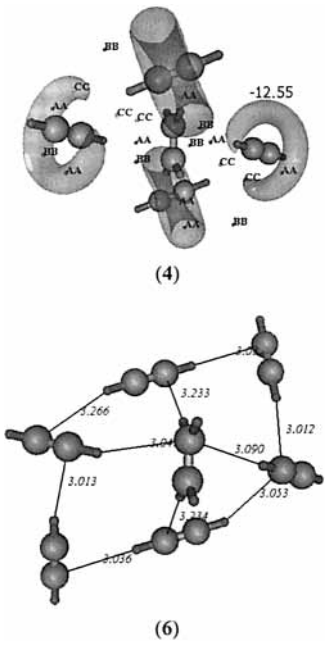

Figure 7. RHF/6-31G(d,p)-optimized geometries of (ethylene)$_m$−(acetylene)$_n$ complexes.

TABLE 7: Interaction Energies and the Relative Energies of Ethylene···(Acetylene)$_n$ Complexes[a]

ethylene···(acetylene)$_n$ complex	RHF/6-311++ G(d, p)	
	ΔE_{int}	ΔE_{rel}
1A	−0.966 (−)	−0.966
2A	−1.780 (−0.806)	−0.973
4	−3.640 (−3.671)	−0.038
6	−6.469 (−6.030)	−0.427

[a] All the values are in kcal/mol. The interaction energies of (acetylene)$_n$ clusters are also shown for a reference in parentheses.

show that ΔE_{rel} is approximately ∼−1 kcal/mol for n = 1 and 2, while in cases of n = 4 and 6 the values are very low, viz. 0.038 and −0.427 kcal/mol, respectively (cf. Table 7). This suggests that interaction energies of ethylene with 4 and 6 acetylene molecules are of the same order as that of acetylene cluster, $(C_2H_2)_n$, n = 4 and 6 (cf. Table 7). Hence the higher clusters of ethylene···(acetylene)$_n$ are energetically rather unfavorable and perhaps not seen in the experiment. It may be noted in passing, however, that ΔE_{rel} for n = 6 case is negative (albeit with small numerical value) indicating that an ethylene molecule may interact somewhat favorably with a hexameric cluster of acetylenes.

The vibrational frequency calculations are performed for some test cases of (ethylene)$_m$···(acetylene)$_n$ complexes, which are shown in Tables S3 and S4 in the Supporting Information. The tables give the details of scaled as well as unscaled vibrational frequencies, and those vibrations with intensities > 20 only are reported. The scaling factors of 0.8929 and 0.9427 (recommended in the GAUSSIAN-94 package[20]) were used at the HF and MP2 levels, respectively, for scaling the frequencies.

Conclusions

We have experimentally observed the 1:1 H···π complex between acetylene and ethylene and have found evidence for two types of complexes; one in which acetylene interacts with the π cloud of ethylene (acetylene acts a proton donor) and another where ethylene acts as a proton donor. Ab initio computations were performed at HF, MP2, and B3LYP levels

to rationalize the experimental results. Computations were also performed to understand the formation of the higher complexes using MESP topography mapping. The 1:2, 1:4, and 1:6 complexes of ethylene−acetylene were identified for which the structures, interaction energies, and frequencies have been derived.

Acknowledgment. Support from the Centre for Development of Advanced Computing (C -DAC), Pune, India, is gratefully acknowledged. We also thank Dr. Shridhar P. Gejji for useful discussions.

Supporting Information Available: Tables and figures providing energies, structures, and vibrational frequencies of the various acetylene−ethylene complexes. This material is available free of charge via the Internet at http://pubs.acs.org.

References and Notes

(1) Pimental, G. C.; McClellan, A. L. *The Hydrogen Bond*; W. H. Freeman: San Francisco, CA, 1960.

(2) Jeffrey, G. A.; Saenger, W. *Hydrogen Bonding in Biological Structures*; Springer: Berlin, 1991.

(3) Jeng, M. H.; DeLaat, A. M.; Ault, B. *J. Phys. Chem*. **1989**, *93*, 3997.

(4) Jeng, M. H.; Ault, B. *J. Phys. Chem*. **1989**, *93*, 5426.

(5) Jeng, M. H.; Ault, B. *J. Phys. Chem*. **1990**, *94*, 1323.

(6) Jeng, M. H.; Ault, B. *J. Phys. Chem*. **1990**, *94*, 4851.

(7) Nishio, M.; Umezawa, Y.; Hirota, M.; Takeuchi, Y. *Tetrahedron* **1995**, *51*, 8665.

(8) Dewar, M. J. S. *J. Chem. Soc*. **1944**, 406.

(9) McDonald, S. A.; Johnson, G. L.; Keelan, B. W.; Andrews, L. *J. Am. Chem. Soc*. **1980**, *102*, 2892.

(10) Jemmis, E. D.; Giju, K. T.; Sundararajan, K.; Sankaran, K.; Vidya, V.; Viswanathan, K. S.; Leszczynski, J. *J. Mol. Struct*. **1999**, *510*, 59.

(11) Engdahl, A.; Nelander, B. *Chem. Phys. Lett.* **1985**, *113*, 49.

(12) Balocchi, F. A.; Williams, J. H.; Klemperer, W. *J. Phys. Chem*. **1983**, *87*, 2079.

(13) Andrews, L.; Johnson, G. L.; Davis, S. R. *J. Phys. Chem*. **1985**, *89*, 1706.

(14) Engdahl, A.; Nelander, B. *J. Phys. Chem*. **1985**, *89*, 2860.

(15) Andrews, L.; Johnson, G. L.; Kelsall, B. J. *J. Chem. Phys*. **1982**, *76*, 5767.

(16) Tsuzuki, S.; Honda, K.; Uchimara, T.; Mikami, M.; Tanabe, K. *J. Am. Chem. Soc*. **2000**, *122*, 3746 and references quoted therein.

(17) Samanta, U.; Chakrabarti, P.; Chandrashekar, J. *J. Phys. Chem*. **1998**, *102*, 8964.

(18) Prichard, D.; Nandi, R. N.; Muenter, J. S. *J. Chem. Phys*. **1988**, *89*, 115.

(19) George, L.; Sankaran, K.; Viswanathan, K. S.; Mathews, C. K. *Appl. Spectrosc.* **1994**, *48*, 7.

(20) Frisch, M. J.; Trucks, G. W.; Schlegel, H. B.; Gill, P. M. W.; Johnson, B. G.; Robb, M. A.; Cheeseman, J. R.; Keith, T.; Petersson, G. A.; Montgomery, J. A.; Raghavachari, K.; Al-Laham, M. A.; Zakrzewski, V. G.; Ortiz, J. V.; Foresman, J. B.; Cioslowski, J.; Stefanov, B. B.; Nanayakkara, A.; Challacombe, M.; Peng, C. Y.; Ayala, P. Y.; Chen, W.; Wong, M. W.; Andres, J. L.; Replogle, E. S.; Gomperts, R.; Martin, R. L.; Fox, D. J.; Binkley, J. S.; Defrees, D. J.; Baker, J.; Stewart, J. J. P.; Head-Gordon, M.; Gonzalez, C.; Pople, J. A. *Gaussian 94*, revision B.3; Gaussian, Inc.: Pittsburgh, PA, 1995.

(21) Schmidt, M. W.; Baldridge, K. K.; Boatz, J. A.; Elbert, S. T.; Gordon, M. S.; Jensen, J. H.; Koseki, S.; Matsunaga, N.; Nguyen, K. A.; Su, S. J.; Windus, T. L.; Dupuis, M.; Montogomery, J. A. GAMESS. *J. Comput. Chem*. **1993**, *14*, 1347.

(22) Bapat, S. V.; Shirsat, R. N.; Gadre, S. R. UNIPROP: Molecular property calculation package developed at the Theoretical Chemistry Group, Department of Chemistry, University of Pune, Pune, India (*Chem. Phys. Lett*. **1992**, *200*, 373).

(23) Limaye, A. C.; Gadre, S. R. UNIVIS-2000: Molecular properties visualization package developed at the Department of Chemistry, University of Pune, Pune, India. See: Limaye, A. C.; Gadre, S. R. *Curr. Sci*., in press.

(24) For an earlier review: (a) Sorocco, E.; Tomasi, J. In *Advances in Quantum Chemistry*; Lowdin, P.-O., Ed.; Academic: New York, 1978; p 116. (b) Politzer, P., Truhlar, D. G., Eds. *Chemical Applications of Atomic and Molecular Electrostatic Potential*; Plenum: New York, 1981. (c) For an inspiring review on MESP applications to biology, see: Pullman, B. *Int. J. Quantum Chem. Quantum Biol. Symp*. **1990**, *17*, 81. For the most recent reviews, see: (d) Gadre, S. R. In *Computational Chemistry: Reviews of Current Trends*; Lesczynski, J., Ed.; World Scientific: Singapore, 2000; Vol. 4. (e) Gadre, S R.; Shirsat, R. N. *Electrostatics of Atoms and Molecules*; Universities Press: Hyderabad, India, 2000; and the references therein.

(25) Becke, A. D. *Phys. Rev*. **1988**, *A38*, 3098.

(26) Becke, A. D. *J. Chem. Phys*. **1993**, *98*, 5648.

(27) Lee, C.; Yang, W.; Parr, R. G. *Phys. Rev*. **1988**, *B37*, 785.

(28) Kline, E. S.; Kafafi, Z. H.; Hauge, R. H.; Margrave, J. L. *J. Am. Chem. Soc.* **1985**, *107*, 7559. (b) Bemish, R. J.; Block, P. A.; Pederson, L. G.; Yang, W.; Miller, R. E. *J. Chem. Phys*. **1993**, *99*, 8585.

(29) Turi, L.; Dannenberg, J. J. *J. Phys. Chem*. **1995**, *99*, 639.

(30) Wong, N.-B.; Cheung, Y.-S.; Wu, D. Y.; Ren, Y.; Wang, X.; Tian, A. M.; Li, W.-K. *J. Mol. Struct*. **2000**, *507*, 153.

(31) Engdahl, A.; Nelander, B. *Chem. Phys. Lett*. **1983**, *100*, 129.